1 **A broad-host range CRISPRi toolkit for silencing gene expression in Burkholderia**

2 Short Title: CRISPRi toolkit for Burkholderia

3 Category: Microbiology

4 Andrew M. Hogan[1], A. S. M. Zisanur Rahman[1], Tasia J. Lightly[1] , Silvia T. Cardona[1,2*].

5

6 [1]Department of Microbiology, University of Manitoba, Winnipeg, MB, Canada.

7 [2]Department of Medical Microbiology & Infectious Disease, University of Manitoba, Winnipeg,

8 Canada.

9 *To whom correspondence should be addressed: Silvia.Cardona@umanitoba.ca

10 Keywords: CRISPR-interference, *Burkholderia*, gene silencing, genetic tool

11

12

13

14

15

Abstract

Genetic tools are critical to dissecting the mechanisms governing cellular processes, from fundamental physiology to pathogenesis. Species of *Burkholderia* have emerged over recent decades as both important opportunistic pathogens in immunocompromised patients and as a rich source of secondary metabolites for biotechnology. With large, high GC content genomes, there are limited tools available for genetic manipulation of *Burkholderia* species. To address this, we have developed CRISPR interference (CRISPRi) technology for gene silencing in *Burkholderia*. Tunable expression was provided by placing a codon-optimized *dcas9* from *Streptococcus pyogenes* under control of a rhamnose-inducible promoter, which was validated by immunoblot. Expression from a multicopy plasmid caused a growth defect; therefore, the mini-CTX single-copy insertion system was used to deliver *dcas9* to the chromosome, resulting in wild-type growth. As a proof of concept, the *paaABCDE* operon controlling genes necessary for phenylacetic acid degradation was targeted by plasmid-borne sgRNAs, resulting in near complete inhibition of growth on phenylacetic acid as a sole carbon source. The utility of CRISPRi to probe other functions at the single cell level was demonstrated knocking down *phbC* and *fliF,* which dramatically reduces polyhydroxybutyrate granule accumulation and motility, respectively. As a hallmark of the mini-CTX system is the broad host-range of integration, we putatively identified 67 genera of Proteobacteria that might be amenable to modification with our CRISPRi toolkit.

38 **Significance statement**

39 Members of the genus *Burkholderia* have potential for biotechnological applications but can also
40 cause disease in humans with a debilitated immune system. The lack of suitable genetic tools to
41 edit *Burkholderia* GC-rich genomes has hampered the exploration of useful capacities and the
42 understanding of pathogenic features. Our CRISPRi tool kit provides a simple and rapid way to
43 silence gene expression to produce an observable phenotype. Linking genes to functions with
44 CRISPRi will facilitate genome editing with the goal of enhancing biotechnological capabilities
45 while reducing *Burkholderia's* pathogenic arsenal.

46

47 **Author contributions**

48 STC conceived the idea and design of the research; AMH designed and cloned the dCas9
49 constructs; AMH and ASMZ designed the sgRNAs, assessed knockdown phenotypes, processed
50 data, and wrote and edited the manuscript; TJL performed qRT-PCR analysis and edited the
51 manuscript; STC supervised the work and provided financial support.

52

53

54

55

56

57 **Introduction**

58 The genus *Burkholderia* comprises a diverse group of Gram-negative bacteria
59 characterized by a remarkable biotechnological potential, with species that can be exploited for
60 bioremediation purposes, production of bioactive compounds, and agricultural growth promotion.
61 Perhaps due to the phylogenetic diversity of the genus, some species of *Burkholderia* can also pose
62 a threat to human health (Eberl and Vandamme, 2016). Within the multiple deep-branching groups
63 of the *Burkholderia* phylogenetic tree (Depoorter et al., 2016), one branch contains the clades
64 known as the *Burkholderia cepacia* complex (Bcc) and the *B. pseudomallei* group. The Bcc group
65 comprises species that cause severe infections in people with the genetic disease cystic fibrosis
66 and other patients with a compromised immune system (Mahenthiralingam et al., 2005). *B.*
67 *cenocepacia* and *B. multivorans* are two relevant species of this group, which are prevalent in
68 cystic fibrosis patients (Kenna et al., 2017). The *B. pseudomallei* group contains the risk group 3
69 members *B. mallei*, *B. pseudomallei*, and its close relative *B. thailandensis*, the last one being a
70 frequent surrogate used in *B. pseudomallei* and *B. mallei* research (Howe et al., 1971). Other
71 branches, such as the *B. xenovorans* group comprise species isolated from diverse environmental
72 sources, like polluted soils, and plant rhizospheres (Depoorter et al., 2016). While species with and
73 without pathogenic potential tend to cluster separately in most phylogenetic trees, the genetic
74 characteristics that define the pathogenic potential of *Burkholderia* are poorly understood.
75 Environmental species can cause serious infections (Nally et al., 2018), calling for caution in the
76 use of *Burkholderia* strains for biotechnological applications. The incomplete understanding of
77 *Burkholderia* pathogenic potential may be related to the limited tools available to link gene to
78 function. Most genome editing methods designed for Gram-negative bacteria are inefficient in

79 *Burkholderia* due in part to their high resistance to the antibiotics used as genetic markers (Rhodes
80 and Schweizer, 2016), and the high GC content of their large genomes.

81 Tools that facilitate controlled gene expression are necessary for interrogation of gene
82 function. Programmable control of gene expression by promoter replacement is a valuable tool to
83 link gene to phenotype (Judson and Mekalanos, 2000). Yet, promoter replacement implies that the
84 natural regulatory circuitry of the target gene is interrupted. Instead, clustered regularly interspaced
85 short palindromic repeats interference (CRISPRi) (Qi et al., 2013) is a method of silencing native
86 gene expression, which is based on a dead Cas9 (dCas9), a nuclease-inactive version of the RNA-
87 guided endonuclease Cas9 (Cho et al., 2013). In CRISPRi, a single guide RNA (sgRNA) designed
88 towards the 5' end of the target gene and the dCas9 protein form an RNA-protein complex that
89 recognizes the target region by base-pairing, and sterically blocks transcription initiation, if
90 targeting the promoter, or elongation if targeting downstream of the promoter, by the RNA
91 polymerase (Figure 1A).

92 Initially developed in *Escherichia coli*, CRISPRi technology has been applied to
93 functionally characterize genomes of a handful of bacteria (Lee et al., 2019; Liu et al., 2017; Peters
94 et al., 2016). To achieve genome-wide control of gene expression a wide range of dCas9 expression
95 levels are necessary, which can be provided by expressing *dcas9* with strong inducible promoters
96 (Peters et al., 2016) or by providing multiple copies of *dcas9* engineered in a plasmid (Lee et al.,
97 2019). Limitations to the success of these genomic efforts are the proteotoxicity of dCas9 when
98 expressed at high levels (Cui et al., 2018) and the necessity of customizing CRISPRi delivery tools
99 across bacteria. Recently, the use of Tn7 transposon mutagenesis, which specifically delivers
100 genetic constructs close to a single *glmS* site (Choi and Schweizer, 2006; Choi et al., 2005) was
101 applied to deliver a mobile CRISPRi system across bacteria (Peters et al., 2019). However, the

102 Tn7 system is less suitable for Burkholderia species as their genomes contain multiple copies of
103 *glmS*, requiring additional steps to confirm the site of chromosomal integration (Choi et al., 2006).

104 In this work, we employ a mini-CTX-derived mutagenesis system (Hoang et al., 2000) to achieve
105 specific chromosomal delivery of *dcas9* in three species of *Burkholderia*, *B. cenocepacia*, *B.*
106 *thailandensis* and *B. multivorans*. Placing the chromosomal copy of *dcas9* under the control of the
107 *E. coli* rhamnose-inducible promoter (Cardona and Valvano, 2005), we demonstrate durable and
108 tunable control of endogenous gene expression, which affects cellular function producing
109 observable phenotypes. We extend the usability of our CRISPRi tool kit by exploring other
110 bacterial genomes for putative mini-CTX insertion sites.

111

112 **Results**

113 *Construction of CRISPRi system*

114 The dCas9 from *Streptococcus pyogenes* has been shown to provide robust gene repression
115 in diverse bacteria (Peters et al., 2016, 2019; Qi et al., 2013); we therefore selected it as our first
116 approach. To function, the dCas9 binds a sgRNA and, by complementary base pairing, is guided
117 to target and silence a gene of interest by sterically blocking the RNA polymerase (Figure 1A) (Qi
118 et al., 2013). However, the genome of *S. pyogenes* has low GC-content (~40%), and from
119 inspection of the *dcas9* gene, we expected poor codon usage in high GC-content organisms such
120 as *Burkholderia* (67%) and subsequently low levels of expression. Indeed, we did not observe
121 detectable levels of dCas9 by immunoblot upon expression of the native gene from *S. pyogenes*
122 from a single copy in the *B. cenocepacia* K56-2 chromosome (Supplemental Figure 1). Upon
123 codon optimization for *B. cenocepacia*, we first introduced the gene into a multicopy plasmid

124 under the control of the rhamnose-inducible promoter (Cardona and Valvano, 2005); however, we
125 observed a severe growth defect upon induction, except at minute concentrations of rhamnose
126 (Supplemental Figure 2A). Growth inhibition was not observed in the vector control
127 (Supplemental Figure 2B) and it remains unclear if the inhibitory effect of dCas9 expression on
128 growth was caused by metabolic load from expression of a large protein in multicopy, or from
129 proteotoxicity.

130 We reasoned a single chromosomal copy of *dcas9* may provide sufficient levels of
131 expression as observed previously (Choudhary et al., 2015; Peters et al., 2016, 2019). Using the
132 mini-CTX system, we introduced a single copy of *dcas9* under control of the rhamnose-inducible
133 promoter into *B. cenocepacia* K56-2 (Supplemental Figure 3A and B). We observed titratable
134 dCas9 expression at various levels of rhamnose by immunoblot (Figure 1B and Supplemental
135 Figure 4A). At rhamnose concentrations up to 0.2% there was no growth defect (Figure 1C)
136 compared to the vector control mutant (Supplemental Figure 4B) Furthermore, dCas9 expression
137 in the presence of a sgRNA with a randomized binding region (sgRNA-non-target) had no effect
138 on growth (Supplemental Figure 4C), demonstrating the current system is well-tolerated in *B.*
139 *cenocepacia* K56-2.

140 *Tunable and durable CRISPRi silencing of paaA strongly suppresses growth on phenylacetic acid*

141 To evaluate the utility of the CRISPRi system for gene repression in *B. cenocepacia* K56-
142 2, we first chose to target the *paaA* gene, which encodes phenylacetate-CoA oxygenase subunit
143 PaaA (Teufel et al., 2010). This gene, and the rest of the *paaABCDE* operon, enable growth with
144 PA as a sole carbon source in *B. cenocepacia* K56-2 (Pribytkova et al., 2014), with the lack of
145 growth being a clearly observable phenotype when the *paaA* gene is disrupted. In addition, as this
146 is the first characterization of CRISPRi in *Burkholderia*, we also wished to assess the effect on

147 repression efficiency when targeting the non-template (NT) and template (T) strands, as previous
148 studies have demonstrated profound differences (Bikard et al., 2013; Qi et al., 2013). We therefore
149 designed five sgRNAs: three sgRNAs targeted the promoter elements and adjacent to the
150 transcription start site (TSS) on the NT strand (sgRNA 1, 2 and 3), one sgRNA targeted near the
151 start codon of *paaA* on the NT strand (sgRNA 4), and one sgRNA targeted near the start codon of
152 *paaA* on the T strand (sgRNA 5) (Figure 2A). For phenotypic characterization of the *paaA* mutants,
153 we used M9 minimal medium with PA (M9+PA) as the sole carbon source. Upon induction of
154 dCas9, the growth of all mutants (except the controls) was suppressed approximately 30-fold
155 (Figure 2B) to the same level of a Δ*paaABCDE* mutant, which is unable to utilize PA as a sole
156 carbon source (Pribytkova et al., 2014). Furthermore, in the absence of rhamnose all of the mutants
157 grew at or near wild-type levels, suggesting that *dcas9* expression is tightly repressed in non-
158 inducing conditions. Interestingly, we did not observe a differential effect of placement of the
159 sgRNA-binding site, as the growth of all mutants was suppressed equally. We also found there to
160 be no difference in control strains; mutants expressing dCas9 and either a guideless or non-
161 targeting sgRNA displayed the same levels of growth.

162 Next, we sought to determine the tunability of our CRISPRi system in *Burkholderia*.
163 Tuning is useful to control the level of transcription inhibition when precision is required, such as
164 in the study of essential genes. To that end, we examined the growth of the dCas9 mutant of *B.*
165 *cenocepacia* K56-2 with the sgRNA1 (targeting *paaA*), using PA as a sole carbon source in the
166 presence of a 2-fold serial dilution of rhamnose. The results showed that our CRISPRi system is
167 tunable, exhibiting growth reduction in a dose-dependent manner with variable repression across
168 sub-saturating rhamnose concentrations (Figure 2C). Intermediate levels of growth were observed
169 in concentrations of rhamnose between 0.00625% and 0.05%. We observed a nearly 30-fold

170 repression in OD_{600nm} at concentrations well below maximum induction as identified by
171 immunoblot, suggesting our system produces more dCas9 than is required for maximum
172 repression. Rhamnose levels beyond 0.2% were intrinsically growth inhibitory precluding their
173 use for inducing gene expression (Figure 2C).

174 Although once rhamnose is removed from the culture, expression of dCas9 is no longer
175 induced, it remained possible that the dCas9 already synthesized may persist and cause long-term,
176 or durable, silencing. To address this, the mutant strains harbouring sgRNAs targeting *paaA,* were
177 grown overnight in rich medium with 0.2% rhamnose, effectively priming the cells with dCas9.
178 When grown in M9+PA with and without rhamnose, we again observed strong repression of
179 growth (~30-fold) in all conditions regardless of the presence of rhamnose in the M9+PA, and at
180 levels similar to the Δ*paaABCDE* mutant (Figure 2D). This suggests that after the inducer is
181 removed, dCas9 is either slowly degraded in K56-2 or is present at high enough levels in the cells
182 for durable repression.

183 *Single-cell analysis reveals an 'all or none' effect in B. cenocepacia K56-2*

184 While at the culture level the effect of CRISPRi is tunable, we further explored the effect
185 of maximum dCas9 induction at the single-cell level. We therefore targeted *fliF,* a gene encoding
186 a transmembrane protein that forms the M ring of the basal body complex of the flagellum. We
187 targeted *fliF* by introducing four sgRNAs designed to bind near the putative promoter and start
188 codon (Supplemental Figure 5A). Our goal was to assess individual cell flagellation as it compares
189 to overall culture swimming motility, and indeed, insertional inactivation of *fliF* completely
190 ablates swimming motility (Supplemental Figure 5B), supporting previous findings (Tomich et al.,
191 2002). While we observed effective inhibition of swimming motility compared to controls in a
192 plate-based assay (approximately 4-fold reduction) (Supplemental Figure 5B and C), we were

193 unable to observe flagella in any of the mutants harbouring gRNAs targeting *fliF* (Supplemental
194 Figure 5D). It is possible that interfering with *fliF* expression rendered fragile flagella that could
195 not remained attached to the cell during the staining process, while still being functional when
196 grown in culture (Komatsu et al., 2016).

197 As a second option, we targeted *phbC,* a gene encoding poly-β-hydroxybutyrate
198 polymerase, an enzyme required for PHB synthesis. To repress *phbC* expression, we designed
199 three sgRNAs to target the region up to 50 bp before the start codon, at the putative promoter site
200 (Figure 3A). Polyhydroxyalkanoate (PHA) granule accumulation was assessed by fluorescence
201 microscopy with Nile red staining after overnight induction with rhamnose. For comparison to a
202 null phenotype, we created a *phbC* insertional mutant (*phbC*::pAH27) which was unable to
203 produce PHA granules (Figure 3B and D). Compared to the wild-type and non-target controls,
204 markedly few cells harbouring sgRNAs targeting *phbC* contained PHA granules, ranging from 17-
205 70% depending on the sgRNA (Figure 3B). sgRNA6 rendered the strongest level of repression,
206 with only 17.1% of cells containing PHA granules in contrast to 86.9% for the wild-type (Figure
207 3B). Interestingly, although few cells possessed PHA granules, the granules were of identical size
208 to those in wild-type cells, averaging 0.65 μm in diameter (Figure 3C and D). As shown by the
209 insertional mutant, inactivation of *phbC* ablates PHA granule accumulation; therefore, the
210 presence of granules of the same size in the dCas9 mutants as in the wild-type is indicative of an
211 'all-or-none' effect in *B. cenocepacia* K56-2, where most cells display the silenced phenotype, but
212 some manage to escape the effect of CRISPRi.

213 *Broad host range of the mini-CTX system extends applicability to other species*

214 Having shown that the *S. pyogenes* dCas9 renders strong gene repression in *B.* cenocepacia
215 K56-2, we next turned our attention to other important species of *Burkholderia.* We introduced the

216 codon-optimized *dcas9* gene into the chromosome of *B. multivorans* ATCC 17616 and targeted
217 the *paaA* and *phbC* genes by designing three sgRNAs for each centered around the putative
218 promoter (Figures 4A and C). Targeted repression of *paaA* by each of the three sgRNAs strongly
219 suppressed growth in M9+PA by approximately 25-fold (Figure 4B), very similar to the activity
220 observed in *B. cenocepacia* K56-2. However, we observed poor expression of dCas9 by
221 immunoblot (Supplemental Figure 6A). Given that the observed phenotype is indicative of
222 effective gene silencing, it is unlikely that the actual expression of dCas9 is as low as detected by
223 immunoblot; however, the basis for this discrepancy is unknown. Expression of dCas9 in the
224 presence of the non-targeting sgRNA did not affect growth in *B. multivorans* ATCC 17616
225 (Supplemental Figure 4C). Following this, targeting *phbC* rendered relatively poor inhibition of
226 PHA granule accumulation with between 35-50% of cells containing PHA granules, depending on
227 the sgRNA (Figure C and D). In contrast to what was seen in *B. cenocepacia* K56-2, we observed
228 granules of reduced size (Figure 4E and F), suggesting there might be compensatory PHA
229 synthesis pathways in *B. multivorans* ATCC 17616.

230 Members of the *B. pseudomallei* group are phylogenetically distinct from the Bcc (Eberl
231 and Vandamme, 2016), but remain of interest due to the ability to cause infection (such as
232 melioidosis and glanders) and for their remarkable capacity for secondary metabolite production
233 (Mao et al., 2017). *B. thailandensis* is a commonly used model for the pathogenic members of the
234 *B. pseudomallei* group, we therefore also introduced the codon-optimized *dcas9* gene into the
235 chromosome of *B. thailandensis* strain E264. When induced with rhamnose, dCas9 was highly
236 expressed (Supplemental Figure 6) and did not impair growth in the presence of a non-targeting
237 sgRNA (Supplemental Figure 4C). Similarly, as for *B. cenocepacia* K56-2 and *B. multivorans*
238 ATCC 17616, we designed three sgRNAs targeting the putative promoters of the *paaA* and *phbC*

239 genes (Figure 5A and C). Upon induction of dCas9 with 0.2% rhamnose, growth of the mutants
240 harbouring the *paaA*-targeting sgRNAs was suppressed in M9+PA to varying levels ranging from
241 3-fold (sgRNA19) to 25-fold (sgRNA20) (Figure 5B). The fact that some sgRNAs yielded only
242 modest repression was not unexpected as the work characterizing the *paaA* promoter done in K56-
243 2 (Pribytkova et al., 2014) would not likely apply as well to E264 as to the more closely related
244 ATCC 17616. Lastly, for the sgRNAs targeting *phbC*, the results mirror those seen in ATCC
245 17616, as depending on the sgRNA there was variation in the percent of cells with PHA granules
246 (10-40%) and the diameter of the granules (overall decrease in size) (Figure 5C and F). Though
247 the exact contributions to PHA synthesis in E264 remain unclear, it has been previously suggested
248 that PhbC is not the only polyhydroxyalkanoate polymerase in E264 (Funston et al., 2017).

249 The integration vector we implemented to deliver *dcas9* to the chromosome of various
250 species of *Burkholderia* relies on the expression of the φCTX integrase and recombination using
251 the plasmid-borne *attP* site with the chromosomal *attB* site. φCTX is a *Pseudomonas*-infecting
252 phage, and the mini-CTX integration system was originally designed for use in *P. aeruginosa*
253 (Hoang et al., 2000). The mini-CTX integration system has been used successfully in other species;
254 however, this has been mostly limited to members of *Burkholderia* (Chapalain et al., 2017; Le
255 Guillouzer et al., 2017). The utility in *Burkholderia* has been comparable to *P. aeruginosa*, in part
256 owing to efficient integration. In the species used in this study, we observed the integration
257 efficiencies to be $6x10^{-7}$ in K56-2, $6x10^{-8}$ in E264, and $5x10^{-9}$ in ATCC 17616 (Supplemental
258 Figure 7A), compared to 10^{-7} to 10^{-8} observed previously in *P. aeruginosa* (Hoang et al., 2000).
259 To further broaden the scope of the applicability of our CRISPRi system, we used NCBI BLAST
260 to search all published genomes for putative *attB* sites. While the full-length *attB* site is 30 nt,
261 integration is known to occur if only the 5' 19 nt are completely complementary, such as for many

262 species of *Burkholderia*. This shorter *attB* site was therefore used as a BLAST query, resulting in
263 1760 hits with 100% alignment (Supplementary Table 4). Enterobacteria were excluded from the
264 search as the pMB1 *oriR* in the mini-CTX system is functional is these species; therefore,
265 integrants cannot be easily isolated. Furthermore, the search parameters were modified to only
266 include species of Proteobacteria. Overall, there were 168 unique species from 67 genera. As
267 expected, the most abundant hit corresponded to species and strains of *Pseudomonas* (480 hits),
268 then followed by *Acinetobacter* (443 hits), *Burkholderia* (276 hits), *Neisseria* (170 hits), and
269 *Ralstonia* (146 hits), with members of the other 62 genera comprising the remaining 245 hits. A
270 summary of the major hits and species of interest (pathogenic, environmental, biotechnological,
271 etc) can be found along with the genomic context in Table 1. We note that the hit table comprises
272 species with both high and low GC-content genomes, and while the GC-rich codon-optimized
273 *dcas9* (in pAH-CTX1-rhadCas9) may be better suited for species with high GC-content genomes,
274 such as those in the families *Pseudomonadaceae* and *Alcaligenaceae*, the native *dcas9* (in pAH-
275 CTX1-rhadCas9-native) may have better functionality in species with low GC-content genomes,
276 such as those in the families *Moraxellaceae* and *Neisseriaceae*.

277 A further consideration for use of our CRISPRi system is that the pFLPe recombinase-
278 expressing plasmids might not be functional in all species. In which case, the *int* and *tet* genes
279 along with the *oriT* and pBM1 *oriR* would not be excised and the mutant would remain resistant
280 to tetracycline. To explore if experiments could be performed in the absence of tetracycline
281 selection, we assessed the stability of the mini-CTX integration in K56-2, ATCC 17616, and E264
282 in serial passages over four days without tetracycline. For all species over the entire experiment
283 we determined CFU counts on agar with and without tetracycline selection and found equal

284 recovery of tetracycline-resistant colonies as total colonies (Supplemental Figure 7B-D),
285 suggesting the integration is stable.

286

287 **Discussion**

288 Genetic tools are necessary to dissect the molecular mechanisms governing cellular
289 processes. Here, we report the development of a CRISPRi system for efficient repression of gene
290 expression in *Burkholderia*. By mobilizing the *dcas9* gene that was codon-optimized for the GC-
291 rich *Burkholderia* on a broad host range mini-CTX1 integration vector, we demonstrate robust,
292 tunable, and durable repression of endogenous genes. While others have shown effective
293 repression using the native *dcas9* gene in *E. coli* (Qi et al., 2013), *B. subtilis* (Peters et al., 2016),
294 *Staphylococcus aureus*, and *Acinetobacter baumannii* (Peters et al., 2019), codon-optimization
295 was a necessary step for K56-2, as expression of the native *dcas9* gene was not detectable in K56-
296 2. Indeed, for expression in species with high GC-content, codon optimization appears to be
297 necessary. In *P. aeruginosa* (66.3% GC) both the *S. pyogenes* dCas9 (Peters et al., 2019) and the
298 *S. pasteurianus* dCas9 (Tan et al., 2018) were not expressed unless first codon-optimized, albeit
299 for *Mycobacterium* (~67% GC) or *Homo sapiens* (optimized at 50.2% GC). Additionally, the *S.*
300 *thermophilus* dCas9 was codon-optimized for *Mycobacterium* for efficient expression in *M.*
301 *tuberculosis* and *M. smegmatis* (Rock et al., 2017).

302 Despite codon-optimizing the *dcas9* gene, we observe a severe growth defect when
303 expressed from a multicopy pBBR1 origin plasmid. At this time, we are unsure if this was caused
304 by a metabolic burden of expressing a large protein from a multicopy plasmid or from direct
305 proteotoxicity. Previous studies have demonstrated that expression of the canonical *S. pyogenes*

306 dCas9 causes toxicity in *M. smegmatis*, *M. tuberculosis* (Rock et al., 2017), and *E. coli* (Cho et al.,
307 2018), which provides rationale for developing a system with low-enough levels of dCas9
308 expression to maintain cell viability without sacrificing repression activity. While this effort has
309 spurred the exploration of alternative dCas9 orthologues (Rock et al., 2017), we found that
310 introducing *dcas9* in single copy in the chromosome provided a balance of repression activity
311 without affecting growth. Furthermore, while other systems display up to 3-fold repression in the
312 absence of inducer (Peters et al., 2016; Tan et al., 2018), our application of the tightly regulated
313 rhamnose-inducible promoter from *E. coli* does not display such a phenomenon in any of the three
314 species tested. Consequently, we suggest this attribute is suited for the investigation of essential
315 genes, as we would predict wild-type growth in the absence of inducer. However, at the cost of
316 apparently negligible uninduced expression, the rhamnose-inducible promoter is incapable of
317 attaining the high levels of maximal expression seen in other systems, such as the xylose-inducible
318 promoter used in the *B. subtilis* CRISPRi library (Peters et al., 2016) (Supplementary Figure 4A).
319 While we did observe increased expression at rhamnose concentrations of 0.5% and 1.0%, it was
320 accompanied by a substantial growth defect. This is similar to the use of the arabinose-inducible
321 promoter in K56-2, in which the 2-3% arabinose necessary to induce maximal expression caused
322 marked changes in cell morphology reminiscent of osmotic stress (Cardona and Valvano, 2005).
323 As a result of the lower levels of maximal expression, it remains possible that our CRISPRi system
324 may not be capable of effectively repressing highly transcribed genes, but this is under
325 investigation. While work by Vigouroux et al. (Vigouroux et al., 2018) suggests that when the
326 sgRNA binding site is saturated with the dCas9:sgRNA complex, fold change in repression is
327 independent of promoter strength; however, the absolute repression of highly active promoters is
328 lower and it is unclear what constitutes saturating levels of dCas9. Furthermore, multiplexing

329 CRISPRi with simultaneous use of more than one sgRNA might reduce the repression at each
330 locus by titrating away dCas9, and this effect may be even more apparent if lower levels of dCas9
331 are present.

332 Critical to fine manipulation of gene expression in precision experiments is tunability. We
333 show that using the rhamnose-inducible promoter can provide intermediate levels of repression
334 and a resulting phenotype of gene depletion rather than complete silencing. Combined with the
335 lack of repression in the uninduced state, we propose that our CRISPRi system will be useful in
336 providing dynamic gene repression. Moreover, the repression caused by dCas9 is durable, as even
337 a full 24 hours after removal of the inducer, we observed the same phenotype as in the cultures
338 grown with inducer. This is in line with previous findings in *Giardia lamblia* (McInally et al.,
339 2019) and *in vitro* (Jones et al., 2017; Sternberg et al., 2014). Interestingly, binding of the
340 dCas9:sgRNA complex to a target is nearly irreversible once the sgRNA has bound with complete
341 complementarity to its target site (Sternberg et al., 2014). Furthermore, this means that the
342 dCas9:sgRNA complex does not follow Michaelis-Menton enzyme kinetics, with each dCas9
343 acting like a single-turnover enzyme that, *in vitro*, can only be removed from the target by strong
344 detergents (Sternberg et al., 2014). *In vivo* however, although the RNA polymerase is largely
345 incapable of displacing the dCas9:sgRNA complex, the DNA replication machinery is not blocked
346 by dCas9. In fact, it has been observed that the dissociation of the dCas9:sgRNA complex
347 correlates well with the generation time in *E. coli* (Jones et al., 2017). This is an important
348 consideration for understanding the durability of growth suppression we observed when using PA
349 as a sole carbon source. When priming the cells by pre-incubation with rhamnose and then placing
350 the cells in M9+PA, they were unable to grow, that is *paaA* became a conditionally essential gene,
351 thereby shutting down cell division and DNA replication. Hence, the DNA replication machinery

352 would not displace the dCas9:sgRNA from the *paaA* gene, resulting in long-term growth
353 suppression. By extension, we predict that strong knockdown of any (conditionally) essential gene
354 that causes a halt in DNA replication would be durable in this manner. This is a useful aspect of
355 CRISPRi that we are investigating further.

356 Although it has been reported that the CRISPRi system is less effective in silencing the
357 gene expression when the template strand (T) is targeted compared to the non-template (NT)
358 strand, our results demonstrated nearly 30-fold repression of the growth irrespective of the *paaA*
359 target strand (Figure 2B). This suggests that the efficiency of the CRISPRi system might not strand
360 specific at all loci, supporting the findings from Howe et al. (Howe et al., 2017). However, this
361 effect might have been masked by the strong repression we observed, as it is difficult to compare
362 across null phenotypes. Additionally, sgRNAs targeting different regions of the 5' region of *paaA*
363 produced a strong 25-30-fold repression in all three species studied here, suggesting that
364 knockdown efficiency is largely unaffected by sgRNA placement on targeting regions overlapping
365 or adjacent to the −35 and −10 promoter elements. possibly resulted from the proximity of the
366 large dCas9:sgRNA complex to the promoter sterically interfering with the RNA polymerase
367 binding. Indeed, the ~160 kDa dCas9 enzyme has an average DNA footprint of 78.1 bp, much
368 larger than most promoter regions (Josephs et al., 2015).

369 Single cell level analysis of our system demonstrated a unimodal 'all or none' effect in
370 K56-2 with ~17% cells escaping the silenced phenotype when targeting *phbC* compared to an
371 insertion mutant, which did not possess any granules. The PHB granules in these cells were of
372 identical diameter to wild type, averaging 0.65µm in diameter. The 'all or none' effect might be
373 attributed to an uneven distribution of the membrane transporter involved in transporting rhamnose
374 into the cell, essentially escaping the rhamnose mediated *dCas9* induction to silence the target gene

375 (Siegele and Hu, 1997). Interestingly, targeting *phbC* in *B. multivorans* ATCC17616 and *B.*
376 *thailandensis* E264 resulted in a mixed phenotype with a reduced number of cells with granules as
377 well as an overall decrease in granule size. Even though some of the cells seemed to have escaped
378 the repression (up to 35% in ATCC17616 and 6% in E264), more than 90% of the cells contained
379 granules of reduced size. The residual presence of PHA granule suggests the existence of an
380 unelucidated PHA synthesis pathways in *B. thailandensis* E264 and *B. multivorans* ATCC 17616,
381 supporting the finding from Funston et al. (Funston et al., 2017).

382 One of the hallmarks of CRISPRi is the broad-range amenability in diverse bacteria,
383 enabling synthetic biology and mechanistic investigations into many dozens of species in
384 innovative ways. We wished to apply our CRISPRi system in this manner and therefore mobilized
385 both the native *dcas9* gene, suitable for low/medium GC-content organisms, and the *dcas9* gene,
386 codon-optimized for GC-rich *Burkholderia*, on the mini-CTX1 integration vector. Our analysis of
387 putative hosts (with *attB* sites near the 3' end of the serine tRNA) identified 168 unique species in
388 67 genera, mostly from the β- and γ-Proteobacteria. Previous works have mobilized *dcas9* on
389 broad host-range integrative plasmids (Peters et al., 2019; Tan et al., 2018); however, both systems
390 use the mini-*Tn*7 system, which has multiple insertion locations in certain genomes, such as many
391 species of *Burkholderia*. Together, our work contributes to the available genetic toolkit for rapid
392 functional analysis of bacteria.

393 **Methods**

394 *Strains, selective antibiotics, and growth conditions*

395 All strains and plasmids are found in Supplemental Table 1. All strains were grown in LB-
396 Lennox medium (Difco). *B. cenocepacia* K56-2 and strains of *E. coli* were grown at 37°C, while

397 *B. thailandensis* E264 and *B. multivorans* ATCC 17616 were grown at 30°C. The following
398 selective antibiotics were used: chloramphenicol (Sigma; 100 µg/mL for *B. cenocepacia,* 20
399 µg/mL for *E. coli*), trimethoprim (Sigma; 100 µg/mL for strains of *Burkholderia*, 50 µg/mL for *E.*
400 *coli*), tetracycline (Sigma; 50 µg/mL for all strains of *Burkholderia*, 20 µg/mL for *E. coli*),
401 kanamycin (250 µg/mL for *B. thailandensis*, 150 µg/mL for *B. multivorans*, 40 µg/mL for *E. coli*),
402 ampicillin (100 µg/mL for *E. coli*), gentamicin (50 µg/mL for all strains of *Burkholderia*).

403 *Construction of pSC-rhadCas9, pAH-CTX1-rhadCas9, pAH-CTX1-rhadCas9-native, and dCas9*
404 *insertional mutants*

405 The endogenous *cas9* gene from *S. pyogenes* has low GC content (averaging 34.1%) and
406 subsequently poor codon usage for GC-rich organisms (http://www.kazusa.or.jp/codon/). The
407 nuclease-inactive variant (*dcas9*) was therefore codon optimized for *B. cenocepacia* by purchasing
408 the optimized gene in two fragments from IDT (2462 bp and 1849 bp, Supplemental table 2), each
409 with 38 bp overlapping regions. Strong, rho-independent terminators were added following the
410 gene. The full-length gene (with terminal *Nde*I and *Hind*III cut sites) was synthesized by overlap-
411 extension PCR using Q5 polymerase with high GC buffer (NEB) and primers 979 and 987
412 (Supplemental Table 2). The first ten rounds of PCR were performed without primers to synthesize
413 the full-length product using the overlap regions; primers were added for the following 25 cycles.
414 The cycle parameters are as follows: 98°C for 30 sec, (98°C for 10 sec, 67.5^{o}C for 20 sec, 72°C for
415 2.5 min)x10 cycles, 72°C for 5 min, 98°C for 30 sec, (98°C for 10 sec, 62.5^{o}C for 20 sec,72 ^{o}C for
416 2.5 min)x25 cycles, 72°C for 10 min. The 4267 bp product was gel-purified (Qiagen) and
417 introduced into pSCrhaB2 by restriction cloning using *Nde*I and *Hind*III (NEB). The resulting
418 plasmid, pSC-rhadCas9, was transformed into *E. coli* DH5α, and trimethoprim-resistant colonies

419 were screened by colony PCR with primers 954 and 955. Triparental mating with *E.* coli
420 MM290/pRK2013 as a helper was performed as previously described (Hogan et al., 2018).

421 Serial restriction cloning was used to introduce the optimized *dcas9* into the mini-CTX1
422 insertion plasmid (Hoang et al., 2000). The rhamnose-inducible promoter from pSC201 (Ortega et
423 al., 2007) was first PCR amplified with Q5 polymerase and primers 976 and 1071, containing
424 *Hind*III and *Spe*I restriction sites, respectively. This fragment was introduced into mini-CTX1, to
425 create pAH-CTX1-rha, and tetracycline-resistant *E. coli* DH5α were screened by colony PCR
426 using primers 957 and 1074. The fragment containing the dCas9 gene was PCR amplified as above,
427 but instead using primers 1072 and 1073, introducing *Spe*I and *Not*I restriction sites, respectively.
428 This fragment was introduced into pAH-CTX1-rha, to create pAH-CTX1-rhadCas9, and
429 tetracycline-resistant *E. coli* DH5α colonies were screened by colony PCR using primers 954 and
430 955.

431 The native (non codon-optimized) *dcas9* was also introduced into pAH-CTX1-rha. The
432 native *dcas9* and transcriptional terminators were PCR amplified from pdCas9-bacteria (Addgene
433 plasmid # 44249) with Q5 polymerase (NEB) using primers 1216 and 1217. The PCR product was
434 cloned into pAH-CTX1-rha (creating pAH-CTX1-rhadcas9-native) using *Not*I and *Spe*I restriction
435 sites then transformed into *E. coli* DH5α. Tetracycline-resistant colonies were screened by PCR
436 using primers 954 and 1218.

437 pAH-CTX1-rha, pAH-CTX1-rhadCas9, and pAH-CTX1-rhadCas9-native were
438 introduced into *Burkholderia* species by triparental mating using *E. coli* MM290/pRK2013 as a
439 helper as above. Tetracycline-resistant colonies were screened by colony PCR using primer 954
440 (for pAH-CTX1-rha) or 1075 (for pAH-CTX1-rhadCas9) or 1219 (for pAH-CTX1-rhadcas9-
441 native) and 1008 (for *B. cenocepacia*), 1167 (for *B. multivorans*), or 1168 (for *B. thailandensis*).

442 While the pFLPe plasmids have been used to remove the tetracycline resistance and
443 integrase genes in other species (Choi et al., 2008), sensitive colonies could not be obtained in *B.*
444 *cenocepacia*. Therefore, the clean deletion method of Flannagan et al was used as previously
445 described (Flannagan et al., 2008). To do this, a fragment with 475 bp overlapping the upstream
446 and downstream regions of the *FRT* sites when pAH-CTX1-rhadCas9 was inserted into the
447 genome (Supplemental Figure 2), was designed and synthesized (IDT) with *Kpn*I and *Eco*RI
448 restriction sites, respectively. The fragment was ligated into pGPI-*Sce*I (Flannagan et al., 2008)
449 via the *Kpn*I and *Eco*RI restriction sites, creating pAH18, and transformed into *E. coli* SY327.
450 Trimethoprim-resistant colonies were screened for the insertion of the fragment with primer 153
451 and 154. pAH18 was introduced into the mutant backgrounds via triparental mating, as described
452 above. Trimethoprim-resistant K56-2 were screened by PCR for both possible integration
453 orientations using primers 154 and 1126, or 153 and 1133. To initiate the second recombination,
454 an *Sce*I-expressing plasmid is required; however, the conventional plasmid, pDAI-*Sce*I, confers
455 tetracycline resistance and could not be selected for in the mutant background. Therefore, the
456 tetracycline resistance cassette was removed by digestion with *Age*I and *Xho*I. The
457 chloramphenicol resistance gene *cat* was PCR amplified from pKD3 (Datsenko and Wanner, 2000)
458 using primers 1084 and 1150, then ligated into the pDAI-*Sce*I backbone and transformed into *E.*
459 *coli* DH5α, creating pAH25-*Sce*I. Chloramphenicol-resistant colonies were screened with primers
460 1091 and 1150. pAH35-*Sce*I was introduced into the mutant backgrounds by triparental mating as
461 described above. Chloramphenicol-resistant colonies were screened for sensitivity to trimethoprim
462 (indicating excision of pAH18) and tetracycline (indicating excision of the genes between the *FRT*
463 sites), and then screened by PCR with primers 1126 and 1133, which bridge the excision.

464 The pFLPe system was used to remove the tetracycline resistance and integrase genes in
465 the dCas9 mutants in *B. multivorans* ATCC 17616 and *B. thailandensis* E264. Triparental mating
466 to introduce pFLPe4 into the strains was performed as for K56-2 above, except 0.2% rhamnose
467 was added to the mating and antibiotic selection plates. Tetracycline-sensitive colonies were
468 screened by PCR using primers 957 and 1194 (for *B. multivorans*) or 1195 (for *B. thailandensis*).
469 pFLPe4 has a temperature-sensitive origin of replication; therefore, mutants were grown overnight
470 in LB without antibiotics at 37°C. Single colonies were then tested for kanamycin sensitivity and
471 then by colony PCR for pFLPe4 using primers 1128 and 1129.

472 *Design and construction of the sgRNA-expressing plasmids*

473 PAM sequences closest to the 5' end of the transcription start site (TSS) were first
474 identified on both the non-template and template strands. We extracted 20-23 nucleotides adjacent
475 to the PAM sequence to design the base-pairing region of the sgRNAs in the following format: 5'-
476 CCN-$N_{(20-23)}$-3' for targeting the non-template strand and 5'$N_{(20-23)}$-NGG-3' for the template
477 strand. To score the specificity and identify off-target binding sites, the 5' end of the 20-23nt
478 variable base-pairing sequences were trimmed one base at a time and the remaining base-pairing
479 region was searched against the appropriate organism's reference genome. This was repeated until
480 only 10 nt was used as a search query. Potential sgRNAs were discarded if off-target sites were
481 discovered in this manner.

482 The expression vector pSCrhaB2 (Cardona and Valvano, 2005) was chosen as the method
483 of sgRNA expression due to the broad host range of the pBBR1 origin of replication. The sgRNA
484 cassette from pgRNA-bacteria (Qi et al., 2013) (Addgene plasmid # 44251) was introduced into
485 pSCrhaB2 by restriction cloning with *Eco*RI and *Hind*III (NEB) to create pSCrhaB2-sgRNA. To
486 remove *rhaS* and *rhaR*, inverse PCR was performed using Q5 polymerase (NEB) and primers 847

487 and 1025. The resulting fragment was ligated by blunt-end ligation using 1μL of PCR product
488 incubated with 0.5 μL *Dpn*I, 0.5 μL T4 polynucleotide kinase, and 0.5 μL T4 ligase (NEB) with
489 quick ligation buffer (NEB) at 37°C for 30 minutes. The resulting plasmid, pSCB2-sgRNA, was
490 screened using primers 781 and 848, which span the ligated junction. Individual sgRNAs were
491 introduced into pSCB2-sgRNA using inverse PCR as previously described (Qi et al., 2013)
492 (Supplemental Table 3).

493 *Construction of the fliF insertional mutant*

494 Inactivation of *fliF* was performed with the mutagenesis system of Flannagan et al.
495 (Flannagan et al., 2007). Briefly, a 322 bp internal fragment of *fliF* was PCR amplified from the
496 K56-2 genome using primers 1156 and 1157 and Q5 polymerase (NEB). The fragment and pGPΩ-
497 Tp were double digested with *Kpn*I and *Eco*RI (NEB) and ligated with T4 ligase (NEB). The
498 resulting plasmid, pAH26, was electroporated into *E. coli* SY327, and trimethoprim-resistant
499 colonies were screened by colony PCR for the *fliF* fragment. Triparental matings were performed
500 as above. Trimethoprim-resistant exconjugants, were screened by motility assay (below).

501 *Construction of the phbC insertional mutant*

502 Inactivation of *phbC* (WQ49_RS30385) was performed as for *fliF*. Briefly, a 328 bp
503 internal fragment of *phbC* was PCR amplified from the K56-2 genome using primers 1196 and
504 1197 and Q5 polymerase (NEB). The plasmid, pAH27, created from ligating the fragment into
505 pGPΩ-Tp using *Kpn*I and *Eco*RI (NEB) restriction sites, was electroporated into *E. coli* SY327
506 and trimethoprim-resistant colonies were screened by colony PCR for the *phbC* fragment.
507 Triparental matings were performed as above, and trimethoprim-resistant exconjugants were
508 screened by staining for polyhydroxyalkanoate granule accumulation (below).

509 *Assays for integration efficiency and stability of the mini-CTX1-based system*

510 To assess integration efficiency, triparental matings were started as above. However, after
511 the mating on LB agar, the pellicles were serially diluted and plated for CFU/mL on LB agar with
512 50 µg/mL gentamicin and LB agar with 50 µg/mL tetracycline and 50 µg/mL gentamicin.

513 To assess stability of the integration, cultures of the dCas9 mutants (containing the
514 tetracycline resistance cassette) were serial passaged over 4 days without antibiotics. Each day, a
515 fresh culture was started by 1:2500 dilution of the previous day's stationary phase culture. In
516 addition, the cultures were serially diluted and plated for CFU/mL on LB agar without antibiotics
517 and LB agar with 50 µg/mL tetracycline.

518 *Growth assay with phenylacetic acid as the sole carbon source*

519 Overnight cultures, started from isolated colonies, of the appropriate strains were washed
520 at 4000x g for 4 minutes and resuspended in PBS (2.7 mM KCl, 136.9 mM NaCl, 1.5 mM KH_2PO_4,
521 8.9 mM Na_2HPO_4, pH 7.4) to remove growth medium. The OD_{600nm} of the cultures was normalized
522 to 0.01 in M9 medium supplemented with 5 mM phenylacetic acid, 100 µg/mL trimethoprim, and
523 0.2% rhamnose as required. The culture was added to wells of a 96-well plate and incubated with
524 continuous shaking at 37°C (for *B. cenocepacia* K56-2) or 30°C (for *B. multivorans* ATCC 17616
525 and *B. thailandensis* E264). The OD_{600nm} of the cultures was measured after 24 hours for *B.*
526 *cenocepacia* K56-2 and *B. multivorans* ATCC 17616, or 48 hours for *B. thailandensis* E264.

527 *Fluorescent microscopy and polyhydroxyalkanoate granule detection*

528 Overnight cultures of the appropriate strains with or without rhamnose were first washed
529 to remove growth medium and resuspended in PBS. Cells were fixed in 3.7% formaldehyde + 1%
530 methanol at room temperature for 10 minutes (*B. cenocepacia* K56-2) or 20 minutes (*B.*

531 *multivorans* ATCC 17616 and *B. thailandensis* E264) then quenched by the addition of an equal
532 volume of 0.5 M glycine. The cells were washed and resuspended in PBS with 0.5 μg/mL Nile
533 Red (Carbosynth) and stained at room temperature in the dark for 20 minutes, after which the cells
534 were washed to remove excess stain and resuspended in PBS. The cells were mounted on 1.5%
535 agarose pads and imaged by fluorescence microscopy at 1000x total magnification on an upright
536 AxioImager Z1 (Zeiss). Nile red was excited at 546/12 nm and detected at 607/33 nm.

537 *Plate-based motility assay*

538 Assays were performed as previously described (Kumar and Cardona, 2016), with some
539 modifications. Briefly, strains were grown on LB agar with the appropriate antibiotics and single
540 colonies were stab-inoculated into motility medium consisting of nutrient broth (Difco) with 0.3%
541 agar. Medium was supplemented with rhamnose (Sigma) as appropriate. Plates were incubated
542 right-side up for 22 hours at 37°C.

543 *Flagellum staining*

544 Staining was performed as previously described (Kumar and Cardona, 2016). Briefly, an
545 overnight culture was rested statically at room temperature for 20 minutes. Gently, a 1 in 10
546 dilution was prepared in water and rested statically for a further 20 minutes. A small drop of the
547 diluted culture was placed on a clean glass slide and rested for 20 minutes. A coverglass was gently
548 applied and one side was flooded with Ryu flagellum stain (Remel), then allowed to dry for 2
549 hours at room temperature. Slides were observed by light microscopy at 1000x total magnification
550 on an upright AxioImager Z1 (Zeiss).

551

552

553 *SDS-PAGE and Immunoblotting*

554 Cells from an overnight culture were subcultured into fresh medium and grown at 37°C
555 (30°C for *B. thailandensis*) to an OD_{600nm} of 0.4, then exposed to various concentrations of
556 rhamnose for 3 hours. Soluble protein was isolated first by sonicating the cells in TNG Buffer (100
557 mM Tris-HCl, 150 mM NaCl, 10% glycerol, pH 7.4) then by centrifugation at 15 000g for 20
558 minutes. Following boiling denaturation in SDS loading buffer (50 mM Tris-HCl, 2% SDS, 0.2%
559 bromophenol blue, 20% glycerol, 100 mM DTT, pH 6.8), samples were run on an 8% Tris/glycine
560 gel. To ensure equal loading, 20 µg protein was loaded per well (as determined by NanoDrop) and
561 gels were run in duplicate (one for immunoblot, and another for Coomassie staining). Protein was
562 transferred by iBlot to a PVDF membrane, blocked in 5% skim milk-TBST (150 mM NaCl, 10
563 mM Tris-HCl, 0.5% Tween-20, pH 7.5) at room temperature for 1 hour, then probed with a 1:2
564 000 dilution of primary α-Cas9 antibody (ThermoFisher 10C11-A12) in 5% skim milk-TBST
565 overnight at 4°C. Following washes, the blot was probed with a 1:20 000 dilution of secondary
566 antibody linked to alkaline phosphatase (ThermoFisher G-21060) in 5% skim milk-TBST for 1
567 hour at room temperature. Protein was detected by incubation with a solution of NBT/BCIP
568 (Roche) as per the manufacturer's protocols.

569

570 **Acknowledgements**

571 This work was financially supported by grants from the Cystic Fibrosis Foundation, Cystic
572 Fibrosis Canada, and the Natural Sciences and Engineering Research Council of Canada (NSERC)
573 to STC; AMH was supported by grants from the Canadian Institutes of Health Research (CIHR)
574 and Cystic Fibrosis Canada.

575 The authors are grateful to Eric Déziel from the Institut National de la Recherche
576 Scientifique – Institut Armand-Frappier for providing the miniCTX1 integration vector.

577

578 **Conflict of Interest Statement**

579 The authors declare no conflict of interest.

580

581 **References**

582 Bikard, D., Jiang, W., Samai, P., Hochschild, A., Zhang, F., and Marraffini, L.A. (2013).
583 Programmable repression and activation of bacterial gene expression using an engineered
584 CRISPR-Cas system. Nucleic Acids Res. *41*, 7429–7437.

585 Cardona, S.T., and Valvano, M.A. (2005). An expression vector containing a rhamnose-inducible
586 promoter provides tightly regulated gene expression in *Burkholderia cenocepacia*. Plasmid *54*,
587 219–228.

588 Chapalain, A., Groleau, M.-C., Le Guillouzer, S., Miomandre, A., Vial, L., Milot, S., and Déziel,
589 E. (2017). Interplay between 4-Hydroxy-3-Methyl-2-Alkylquinoline and N-Acyl-Homoserine
590 Lactone Signaling in a Burkholderia cepacia Complex Clinical Strain. Front. Microbiol. *8*, 1021.

591 Cho, S., Choe, D., Lee, E., Kim, S.C., Palsson, B., and Cho, B.-K. (2018). High-Level dCas9
592 Expression Induces Abnormal Cell Morphology in Escherichia coli. ACS Synth. Biol.

593 Cho, S.W., Kim, S., Kim, J.M., and Kim, J.-S. (2013). Targeted genome engineering in human
594 cells with the Cas9 RNA-guided endonuclease. Nat. Biotechnol. *31*, 230–232.

595 Choi, K.-H., and Schweizer, H.P. (2006). mini-Tn7 insertion in bacteria with single attTn7 sites:
596 example Pseudomonas aeruginosa. Nat. Protoc. *1*, 153–161.

597 Choi, K.H., Gaynor, J.B., White, K.G., Lopez, C., Bosio, C.M., Karkhoff-Schweizer, R.R., and
598 Schweizer, H.P. (2005). A Tn7-based broad-range bacterial cloning and expression system.
599 Nat.Methods *2*, 443–448.

600 Choi, K.H., DeShazer, D., and Schweizer, H.P. (2006). mini-Tn7 insertion in bacteria with
601 multiple glmS-linked attTn7 sites: example *Burkholderia mallei* ATCC 23344. Nat. Protoc. *1*,
602 162–169.

603 Choi, K.H., Mima, T., Casart, Y., Rholl, D., Kumar, A., Beacham, I.R., and Schweizer, H.P.
604 (2008). Genetic tools for select-agent-compliant manipulation of *Burkholderia pseudomallei*.
605 Appl. Environ. Microbiol. *74*, 1064–1075.

606 Choudhary, E., Thakur, P., Pareek, M., and Agarwal, N. (2015). Gene silencing by CRISPR
607 interference in mycobacteria. Nat. Commun. *6*, ncomms7267.

608 Cui, L., Vigouroux, A., Rousset, F., Varet, H., Khanna, V., and Bikard, D. (2018). A CRISPRi
609 screen in E. coli reveals sequence-specific toxicity of dCas9. Nat. Commun. *9*, 1912.

610 Darling, P., Chan, M., Cox, A.D., and Sokol, P.A. (1998). Siderophore production by cystic
611 fibrosis isolates of *Burkholderia cepacia*. Infect. Immun. *66*, 874–877.

612 Datsenko, K.A., and Wanner, B.L. (2000). One-step inactivation of chromosomal genes in
613 *Escherichia coli* K-12 using PCR products. Proc Natl Acad Sci U A *97*, 6640–6645.

614 Depoorter, E., Bull, M.J., Peeters, C., Coenye, T., Vandamme, P., and Mahenthiralingam, E.
615 (2016). Burkholderia: an update on taxonomy and biotechnological potential as antibiotic
616 producers. Appl. Microbiol. Biotechnol. *100*, 5215–5229.

617 Eberl, L., and Vandamme, P. (2016). Members of the genus *Burkholderia*: good and bad guys.
618 F1000Research *5*, 1007.

619 Figurski, D.H., and Helinski, D.R. (1979). Replication of an origin-containing derivative of
620 plasmid RK2 dependent on a plasmid function provided in trans. Proc. Natl. Acad. Sci. U. S. A.
621 *76*, 1648–1652.

622 Flannagan, R.S., Aubert, D., Kooi, C., Sokol, P.A., and Valvano, M.A. (2007). Burkholderia
623 cenocepacia requires a periplasmic HtrA protease for growth under thermal and osmotic stress and
624 for survival *in vivo*. Infect. Immun. *75*, 1679–1689.

625 Flannagan, R.S., Linn, T., and Valvano, M.A. (2008). A system for the construction of targeted
626 unmarked gene deletions in the genus *Burkholderia*. Environ. Microbiol. *10*, 1652–1660.

627 Funston, S.J., Tsaousi, K., Smyth, T.J., Twigg, M.S., Marchant, R., and Banat, I.M. (2017).
628 Enhanced rhamnolipid production in Burkholderia thailandensis transposon knockout strains
629 deficient in polyhydroxyalkanoate (PHA) synthesis. Appl. Microbiol. Biotechnol. *101*, 8443–
630 8454.

631 Hoang, T.T., Kutchma, A.J., Becher, A., and Schweizer, H.P. (2000). Integration-proficient
632 plasmids for Pseudomonas aeruginosa: site-specific integration and use for engineering of reporter
633 and expression strains. Plasmid *43*, 59–72.

634 Hogan, A.M., Scoffone, V.C., Makarov, V., Gislason, A.S., Tesfu, H., Stietz, M.S., Brassinga,
635 A.K.C., Domaratzki, M., Li, X., Azzalin, A., et al. (2018). Competitive Fitness of Essential Gene
636 Knockdowns Reveals a Broad-Spectrum Antibacterial Inhibitor of the Cell Division Protein FtsZ.
637 Antimicrob. Agents Chemother. *62*.

638 Howe, C., Sampath, A., and Spotnitz, M. (1971). The pseudomallei group: a review. J. Infect. Dis.
639 *124*, 598–606.

640 Howe, F.S., Russell, A., Lamstaes, A.R., El-Sagheer, A., Nair, A., Brown, T., and Mellor, J.
641 (2017). CRISPRi is not strand-specific at all loci and redefines the transcriptional landscape. ELife
642 *6*.

643 Jones, D.L., Leroy, P., Unoson, C., Fange, D., Ćurić, V., Lawson, M.J., and Elf, J. (2017). Kinetics
644 of dCas9 target search in Escherichia coli. Science *357*, 1420–1424.

645 Josephs, E.A., Kocak, D.D., Fitzgibbon, C.J., McMenemy, J., Gersbach, C.A., and Marszalek, P.E.
646 (2015). Structure and specificity of the RNA-guided endonuclease Cas9 during DNA
647 interrogation, target binding and cleavage. Nucleic Acids Res. *43*, 8924–8941.

648 Judson, N., and Mekalanos, J.J. (2000). TnAraOut, a transposon-based approach to identify and
649 characterize essential bacterial genes. Nat Biotechnol *18*, 740–745.

650 Kenna, D.T.D., Lilley, D., Coward, A., Martin, K., Perry, C., Pike, R., Hill, R., and Turton, J.F.
651 (2017). Prevalence of Burkholderia species, including members of Burkholderia cepacia complex,
652 among UK cystic and non-cystic fibrosis patients. J. Med. Microbiol. *66*, 490–501.

653 Komatsu, H., Hayashi, F., Sasa, M., Shikata, K., Yamaguchi, S., Namba, K., and Oosawa, K.
654 (2016). Genetic analysis of revertants isolated from the rod-fragile fliF mutant of Salmonella.
655 Biophys. Physicobiology *13*, 13–25.

656 Kumar, B., and Cardona, S.T. (2016). Synthetic Cystic Fibrosis Sputum Medium Regulates
657 Flagellar Biosynthesis through the flhF Gene in *Burkholderia* cenocepacia. Front. Cell. Infect.
658 Microbiol. *6*, 65.

659 Le Guillouzer, S., Groleau, M.-C., and Déziel, E. (2017). The Complex Quorum Sensing Circuitry
660 of Burkholderia thailandensis Is Both Hierarchically and Homeostatically Organized. MBio *8*.

661 Lee, H.H., Ostrov, N., Wong, B.G., Gold, M.A., Khalil, A.S., and Church, G.M. (2019). Functional
662 genomics of the rapidly replicating bacterium Vibrio natriegens by CRISPRi. Nat. Microbiol.

663 Liu, X., Gallay, C., Kjos, M., Domenech, A., Slager, J., van Kessel, S.P., Knoops, K., Sorg, R.A.,
664 Zhang, J.-R., and Veening, J.-W. (2017). High-throughput CRISPRi phenotyping identifies new
665 essential genes in Streptococcus pneumoniae. Mol. Syst. Biol. *13*, 931.

666 Mahenthiralingam, E., Urban, T.A., and Goldberg, J.B. (2005). The multifarious, multireplicon
667 *Burkholderia cepacia* complex. Nat. Rev. Microbiol. *3*, 144–156.

668 Mao, D., Bushin, L.B., Moon, K., Wu, Y., and Seyedsayamdost, M.R. (2017). Discovery of scmR
669 as a global regulator of secondary metabolism and virulence in *Burkholderia thailandensis* E264.
670 Proc. Natl. Acad. Sci. U. S. A. *114*, E2920–E2928.

671 McInally, S.G., Hagen, K.D., Nosala, C., Williams, J., Nguyen, K., Booker, J., Jones, K., and
672 Dawson, S.C. (2019). Robust and stable transcriptional repression in Giardia using CRISPRi. Mol.
673 Biol. Cell *30*, 119–130.

674 Miller, V.L., and Mekalanos, J.J. (1988). A novel suicide vector and its use in construction of
675 insertion mutations: osmoregulation of outer membrane proteins and virulence determinants in
676 *Vibrio cholerae* requires *toxR*. J. Bacteriol. *170*, 2575–2583.

677 Nally, E., Groah, S.L., Pérez-Losada, M., Caldovic, L., Ljungberg, I., Chandel, N.J., Sprague, B.,
678 Hsieh, M.H., and Pohl, H.G. (2018). Identification of Burkholderia fungorum in the urine of an
679 individual with spinal cord injury and augmentation cystoplasty using 16S sequencing: copathogen
680 or innocent bystander? Spinal Cord Ser. Cases *4*, 85.

681 Ortega, X.P., Cardona, S.T., Brown, A.R., Loutet, S.A., Flannagan, R.S., Campopiano, D.J.,
682 Govan, J.R., and Valvano, M.A. (2007). A putative gene cluster for aminoarabinose biosynthesis
683 is essential for *Burkholderia cenocepacia* viability. J. Bacteriol. *189*, 3639–3644.

684 Peters, J.M., Colavin, A., Shi, H., Czarny, T.L., Larson, M.H., Wong, S., Hawkins, J.S., Lu, C.H.,
685 Koo, B.M., Marta, E., et al. (2016). A comprehensive, CRISPR-based functional analysis of
686 essential genes in bacteria. Cell *165*, 1493–1506.

687 Peters, J.M., Koo, B.-M., Patino, R., Heussler, G.E., Hearne, C.C., Qu, J., Inclan, Y.F., Hawkins,
688 J.S., Lu, C.H.S., Silvis, M.R., et al. (2019). Enabling genetic analysis of diverse bacteria with
689 Mobile-CRISPRi. Nat. Microbiol. *4*, 244.

690 Pribytkova, T., Lightly, T.J., Kumar, B., Bernier, S.P., Sorensen, J.L., Surette, M.G., and Cardona,
691 S.T. (2014). The attenuated virulence of a Burkholderia cenocepacia paaABCDE mutant is due to
692 inhibition of quorum sensing by release of phenylacetic acid. Mol. Microbiol. *94*, 522–536.

693 Qi, L.S., Larson, M.H., Gilbert, L.A., Doudna, J.A., Weissman, J.S., Arkin, A.P., and Lim, W.A.
694 (2013). Repurposing CRISPR as an RNA-guided platform for sequence-specific control of gene
695 expression. Cell *152*, 1173–1183.

696 Rhodes, K.A., and Schweizer, H.P. (2016). Antibiotic resistance in Burkholderia species. Drug
697 Resist. Updat. *28*, 82–90.

698 Rock, J.M., Hopkins, F.F., Chavez, A., Diallo, M., Chase, M.R., Gerrick, E.R., Pritchard, J.R.,
699 Church, G.M., Rubin, E.J., Sassetti, C.M., et al. (2017). Programmable transcriptional repression
700 in mycobacteria using an orthogonal CRISPR interference platform. Nat. Microbiol. *2*, 16274.

701 Siegele, D.A., and Hu, J.C. (1997). Gene expression from plasmids containing the araBAD
702 promoter at subsaturating inducer concentrations represents mixed populations. Proc Natl Acad
703 Sci U A *94*, 8168–8172.

704 Sternberg, S.H., Redding, S., Jinek, M., Greene, E.C., and Doudna, J.A. (2014). DNA interrogation
705 by the CRISPR RNA-guided endonuclease Cas9. Nature *507*, 62–67.

706 Tan, S.Z., Reisch, C.R., and Prather, K.L.J. (2018). A Robust CRISPRi Gene Repression System
707 inPseudomonas. J. Bacteriol. *200*, e00575-17.

708 Teufel, R., Mascaraque, V., Ismail, W., Voss, M., Perera, J., Eisenreich, W., Haehnel, W., and
709 Fuchs, G. (2010). Bacterial phenylalanine and phenylacetate catabolic pathway revealed. Proc.
710 Natl. Acad. Sci. U. S. A. *107*, 14390–14395.

711 Tomich, M., Herfst, C.A., Golden, J.W., and Mohr, C.D. (2002). Role of flagella in host cell
712 invasion by Burkholderia cepacia. Infect. Immun. *70*, 1799–1806.

713 Vigouroux, A., Oldewurtel, E., Cui, L., Bikard, D., and Teeffelen, S. van (2018). Tuning dCas9's
714 ability to block transcription enables robust, noiseless knockdown of bacterial genes. Mol. Syst.
715 Biol. *14*, e7899.

716 **Table 1.** Putative host range of the mini-CTX system and genomic context of selected hit sites

Class	Order	Family	Genus and Species	Strain	%GC	tRNA^{Ser} ( ) Genomic Context
Gammaproteobacteria	Pseudomonadales	Pseudomonadaceae	*Pseudomonas aeruginosa*	PAO1	66.6	PA2603 PA2603.1 PA2604
			Pseudomonas fluorescens	NCTC 10783	65.9	EL286_RS07725 EL286_RS07730 EL286_RS07735
			Pseudomonas mendocina	NK-01	64.7	MDS_RS12060 MDS_RS12065 MDS_RS12070
		Moraxellaceae	*Acinetobacter baumannii*	ATCC 17978	39	AUO97_RS02215 AUO97_RS02215 AUO97_RS02220 fadH AUO97_RS12570 AUO97_RS12570
			Acinetobacter nosocomialis	NCTC 8102	38.7	DIW83_RS04465 DIW83_RS04470 DIW83_RS04475 DIW83_RS13465 DIW83_RS13470 fadH
	Xanthomonadales	Xanthomonadaceae	*Xylella fastidiosa*	M12	51.9	XFASM12_RS11770 XFASM12_RS07835 XFASM12_RS07840
Betaproteobacteria	Burkholderiales	Alcaligenaceae	*Achromobacter xylosoxidans*	NCTC 10808	67.4	DQO23_RS06440 DQO23_RS06445 DQO23_RS06450
			Bordatella bronchiseptica	D448	68.1	CS344_RS23895 CS344_RS23900 CS344_RS23905
			Alcaligenes faecalis	DSM 30030	56.6	CPY64_RS11990 CPY64_RS11995 CPY64_RS12000
		Burkholderiaceae	*Ralstonia pickettii*	DTP0602	65.9	N234_04430 N234_04435 N234_04440
			Burkholderia cenocepacia	K56-2	67	WQ49_RS02320 WQ49_RS02325 WQ49_RS02330
			Burkholderia multivorans	ATCC 17616	66.7	BMULJ_RS32145 BMULJ_RS04140 BMULJ_RS04145
			Burkholderia thailandensis	E264	67.7	BTH_RS32930 BTH_RS20275 BTH_RS20280
			Burkholderia mallei	NCTC 10229	68.5	BMA10229_RS30760 BMA10229_RS21960 BMA10229_RS21965
			Burkholderia pseudomallei	NCTC 13178	67.9	BBJ_RS32360 BBJ_RS01310 BBJ_RS01315
			Burkholderia oklahomensis	EO147	66.9	DM82_RS11255 DM82_RS11260 DM82_RS11265
			Cupriavidus necator	NH9	65.5	BJN34_RS05080 BJN34_RS05085 BJN34_RS05090
			Pandoraea apista	AU2161	62.6	AA956_RS16715 AA956_RS16720 AA956_RS25505
			Lautropia mirabilis	NCTC 12852	65.5	EL249_RS10610 EL249_RS10615 EL249_RS10620
		Oxalobactericeae	*Collimonas fungivorans*	Ter6	59	CFter6_RS10510 CFter6_RS10515 CFter6_RS25055
		Commamonadaceae	*Rhodoferax antarcticus*	DSM 24876	58.9	RA876_RS18910 RA876_RS18915 RA876_RS18920
			Polaromonas naphthalenivorans	CJ2	61.7	PNAP_RS04840 PNAP_RS04845 *ureG*
	Neisseriales	Neisseriaceae	*Neisseria meningitidis*	NCTC 10026	51.4	EL323_RS06235 EL323_RS06240 *yaaA*
			Neisseria gonorrheae	NCTC 13484	52.5	EL177_RS06240 EL177_RS06245 *yaaA*
			Neisseria sicca	FDAARGOS_260	50.9	A6J88_RS26510 A6J88_RS26515 A6J88_RS26520
			Chromobacterium violaceum	CV1197	65.6	CR207_RS10565 CR207_RS10570 CR207_RS10575
	Nitrosomonadales	Nitrosomonadaceae	*Nitrosomonas communis*	Nm2	44.7	AAW31_RS16120 AAW31_RS16125 AAW31_RS16130
Hydrogenophilalia	Hydrogenophilales	Hydrogenophilaceae	*Hydrogenophilus thermoluteolus*	TH-1	61.7	HPTL_RS08770 HPTL_RS08775 HPTL_RS08780
Alphaproteobacteria	Rhodospirillales	Rhodospirillaceae	*Haematospirillum jordaniae*	H5569	55.6	AY555_RS08435 AY555_RS08440 AY555_RS08445

717

718

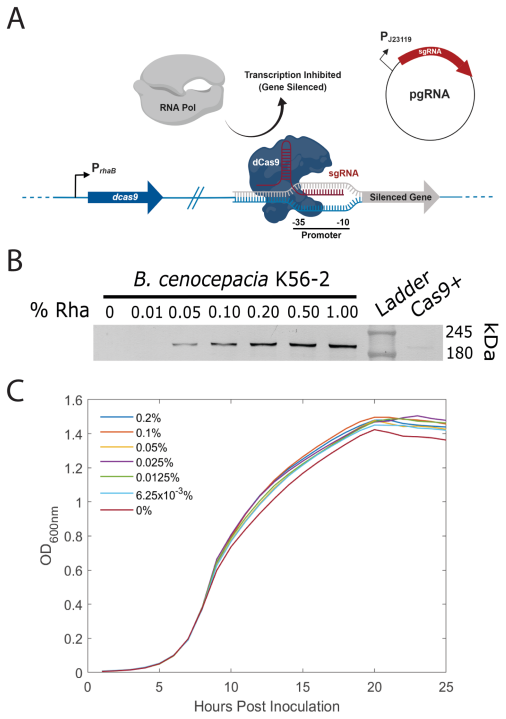

Figure 1. Development of CRISPRi in *B. cenocepacia* K56-2. A) The CRISPRi toolkit is composed of a chromosomal codon-optimized version of the *S. pyogenes dcas9* and plasmid pgRNA harboring the sgRNA under the control of the constitutive promoter P_{J23119}. B) dCas9 is dynamically expressed from the chromosome of K56-2 by rhamnose. Cells were grown to OD_{600nm} of 0.6 then induced with rhamnose for three hours. Soluble protein was harvested and run on an 8% SDS gel. dCas9 was detected by an α-dCas9 antibody then by a 2° antibody linked to alkaline phosphatase C) Chromosomally-encoded dCas9 induced with rhamnose up to 0.2% does not affect growth in K56-2.

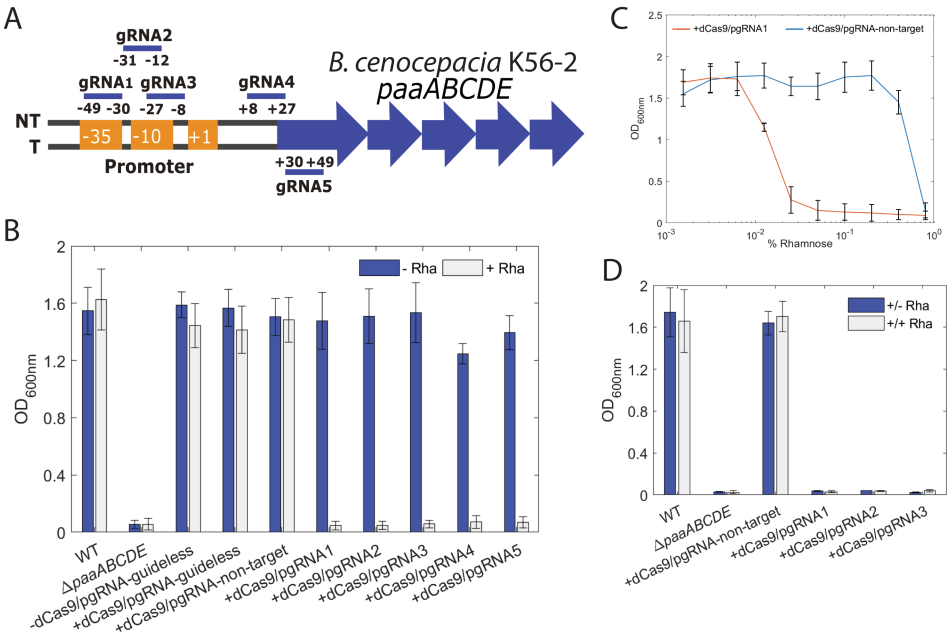

Figure 2. Targeting *paaA* with CRISPRi effectively suppresses growth in phenylacetic acid as the sole carbon source in *B. cenocepacia* K56-2. A) Positions of the sgRNAs targeting different regions upstream of and on *paaA*. sgRNAs 1, 2, and 3 were designed to target the promoter elements (-35 and -10 boxes) on the non-template (NT) strand. gRNA4 targeted the start codon on the NT strand and gRNA5 targeted the downstream region adjacent to the start codon on the T strand. B) CRISPRi blocks transcription in a strand non-specific manner. WT, a mutant of the *paaABCDE* operon (Δ*paaABCDE*), K56-2::CTX1-rha (-dCas9) and K56-2::dCas9 (+dCas9) harboring pgRNA with or without specific gRNAs were grown for 24 hours in minimal medium with PA (M9+PA) without (-Rha) or with 0.2% rhamnose (+Rha). C) Expression of the dCas9 can be controlled by varying the amount of inducer added to the medium, providing tunability to the CRISPRi system. However, high level induction of dCas9 with rhamnose (0.4% and beyond) was lethal for the non-genome targeting mutant expressing dCas9. D) Cells were grown overnight in LB medium with 0.2% rhamnose to induce expression of dCas9. Then cells were transferred to fresh medium and grown with (+/+ Rha) and without (+/- Rha) 0.2% rhamnose. All the values are the average of three independent biological replicates; error bars represent arithmetic mean ± SD.

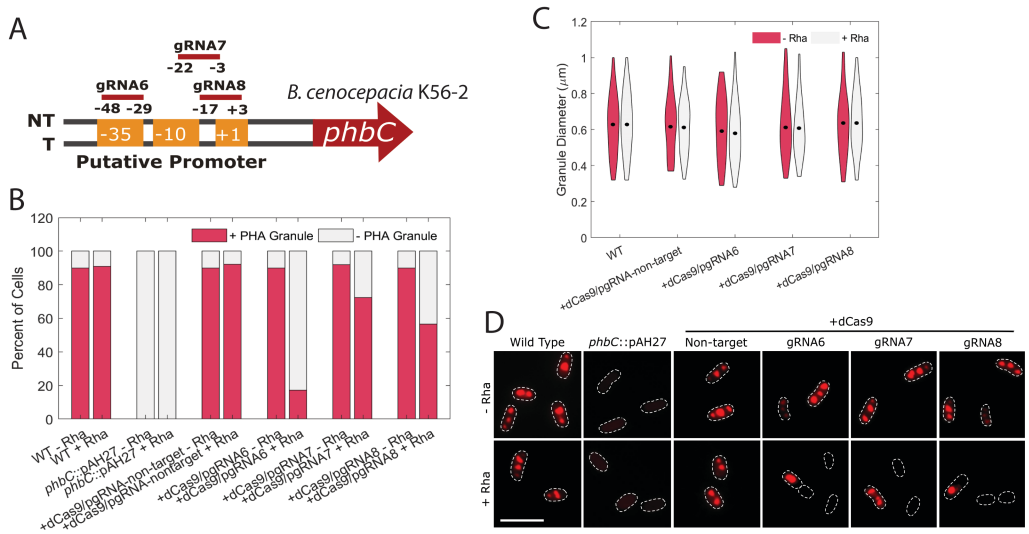

Figure 3. Targeting *phbC* with CRISPRi reduces polyhydroxyalkanoate (PHA) granule accumulation in K56-2. A) Positions of the sgRNAs targeting different regions upstream of *phbC*. sgRNAs 6, 7, and 8 were designed to target the promoter elements (-35 and -10 boxes) on the non-template (NT) strand. B) CRISPRi reduces but does not completely abrogate the number of cells with PHA granules. WT, an insertional mutant of the *phbC* gene (*phbC::*pAH27), K56-2::CTX1-rha (-dCas9) and K56-2::dCas9 (+dCas9) harboring pgRNA with or without specific gRNAs were grown overnight without (-Rha) or with 0.2% rhamnose (+Rha). Cells were washed and stained with Nile Red, and observed by fluorescence microscopy. One to two-hundred cells were counted and the % of cells with PHA granules was calculated. C) PHA granules that remain are identical to those in the WT. Strains were grown and processed as for B and the diameter of the PHA granules was measured. Thicker areas of the violin bars represent more granules with that diameter. The mean in each condition is shown by a black dot. D) The strains were grown and processed as for B). Dashes indicate cell boundaries and the scale bar is 5 μm.

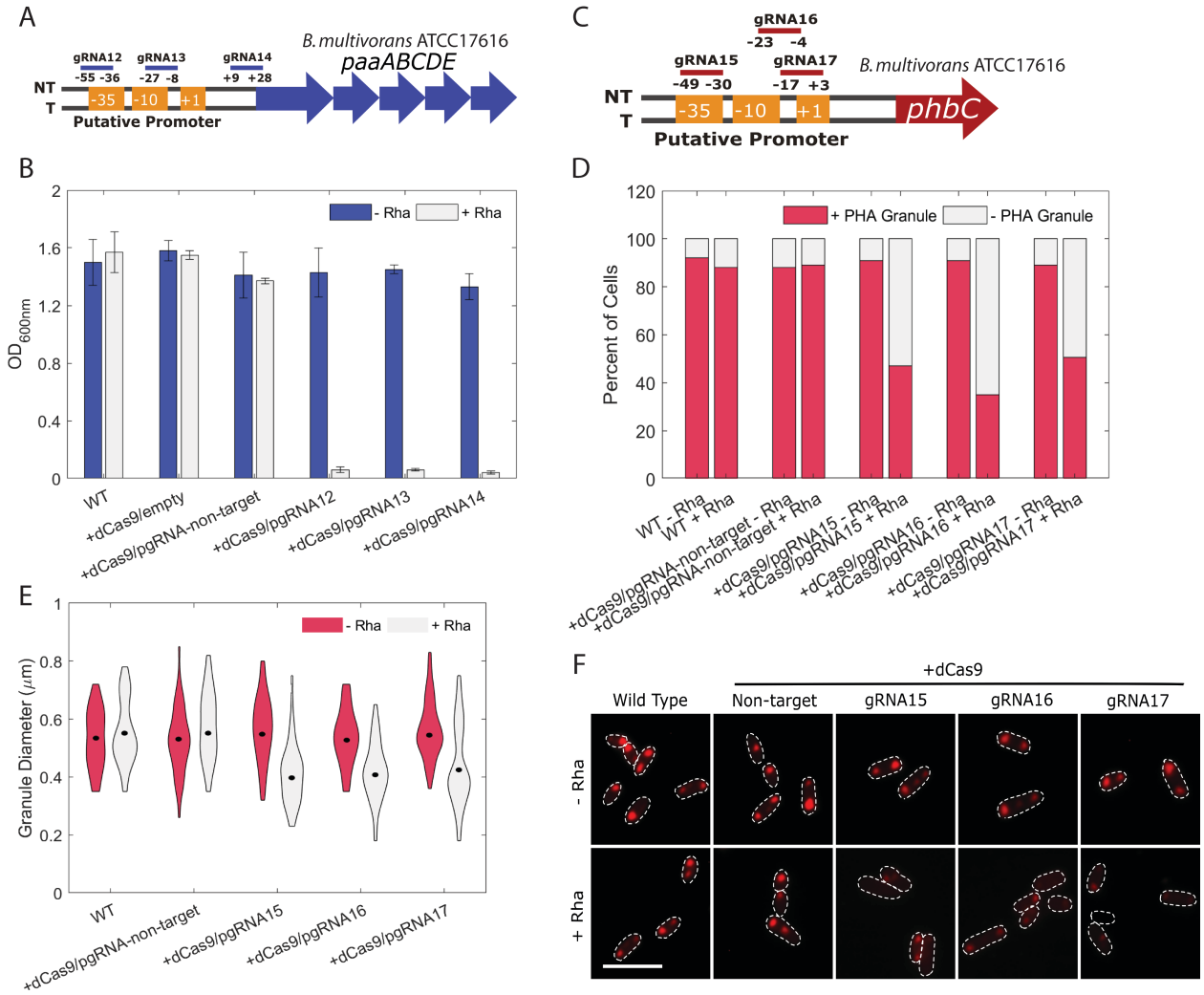

Figure 4. CRISPRi in *B. multivorans* ATCC17616 effectively represses *paaA* and *phbC*. A) Positions of the sgRNAs targeting upstream regions of *paaA*. sgRNAs 12 and 13 were designed to target the -35 and -10 boxes of the promoter, while sgRNA14 targeted the 5' region of the ORF. All sgRNAs targeted the NT strand. B) Targeting *paaA* suppressed growth on PA as a sole carbon source. WT, ATCC 17616::dCas9 (+dCas9) with or without sgRNAs in A) were grown for 24 hours in M9+PA without (-Rha) or with 0.2% rhamnose (+Rha). C) Positions of the sgRNAs targeting upstream regions of *phbC*. All sgRNAs were designed to target the -35 or -10 elements of the promoter on the NT strand. D) Targeting *phbC* reduces the overall number of cells with

773 PHA granules. Strains were grown overnight without (-Rha) or with 0.2% rhamnose (+Rha). Cells
774 were washed and stained with Nile Red, and observed by fluorescence microscopy. One to two-
775 hundred cells were counted and the % of cells with PHA granules was calculated. E) PHA granules
776 that remain are smaller than those in the WT. Strains were grown and processed as for D); however,
777 the diameter of the PHA granules was measured, with thicker areas representing more granules
778 with that diameter. The mean in each condition is shown by a black dot. F) The strains were grown
779 and processed as for D). Dashes indicate cell boundaries and the scale bar is 5 μm.

780

781

782

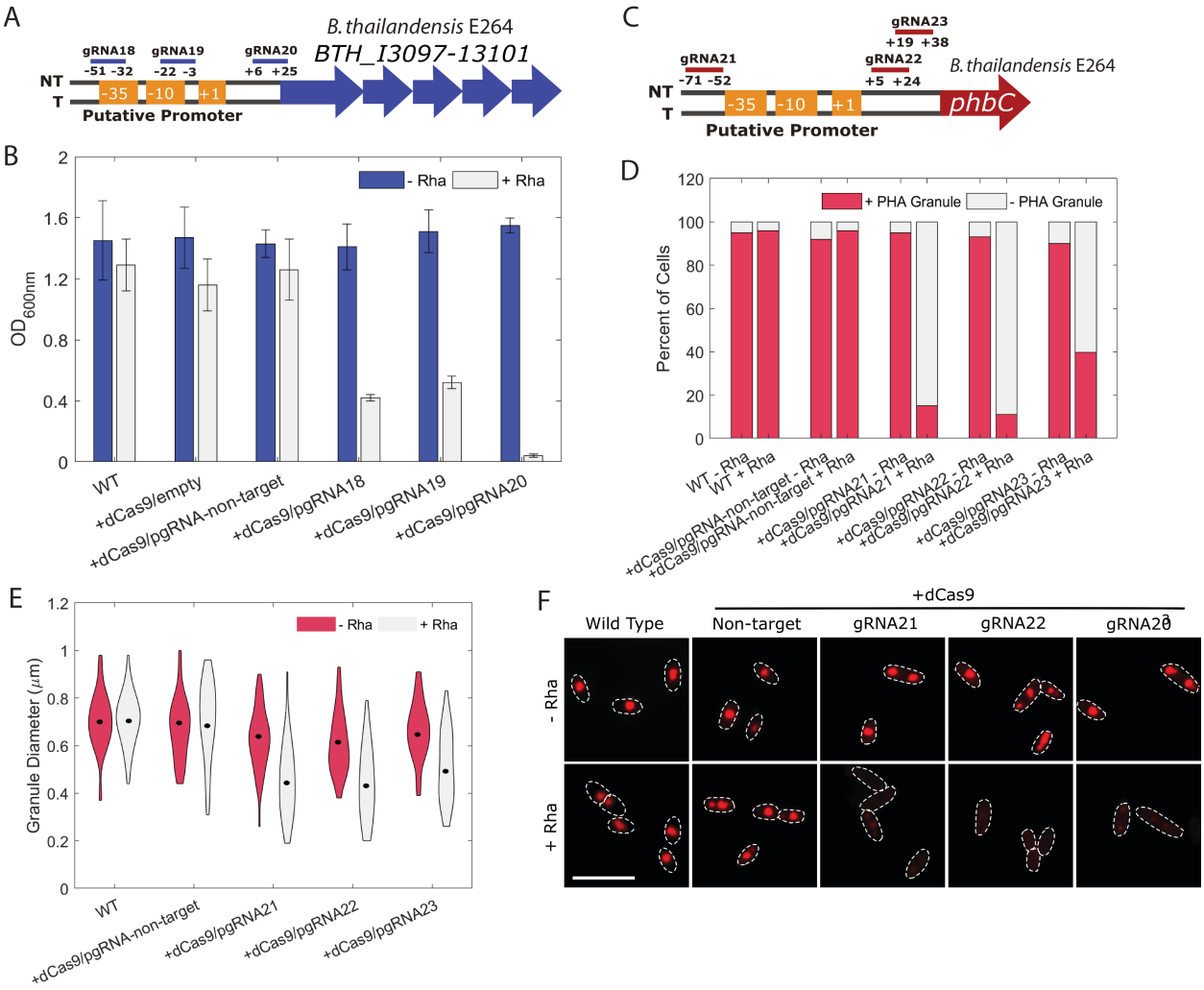

Figure 5. CRISPRi in *B. thailandensis* E264 effectively represses *paaA* (BTH_I3097) and *phbC*. Positions of the sgRNAs targeting upstream regions of *paaA* (BTH_I3097). sgRNAs 18 and 19 were designed to target the -35 and -10 boxes of the promoter, while sgRNA 20 targeted the 5' region of the ORF. All sgRNAs targeted the NT strand. B) Targeting *paaA* suppressed growth on PA as a sole carbon source. WT, E264::dCas9 (+dCas9) with or without sgRNAs in A) were grown for 48 hours in M9+PA without (-Rha) or with 0.2% rhamnose (+Rha). C) Positions of the sgRNAs targeting regions of *phbC*. sgRNA 21 targeted just upstream of the -35 box, sgRNA22 and 23 targeted just downstream of the -10 box, all on the NT strand. D) Targeting *phbC* reduces the

793 overall number of cells with PHA granules. Strains were grown overnight without (-Rha) or with
794 0.2% rhamnose (+Rha). Cells were washed and stained with Nile red, and observed by
795 fluorescence microscopy. One to two-hundred cells were counted and the % of cells with PHA
796 granules was calculated. E) PHA granules that remain are smaller than those in the WT. Strains
797 were grown and processed as for D); however, the diameter of the PHA granules was measured,
798 with thicker areas representing more granules with that diameter. The mean in each condition is
799 shown by a black dot. F) The strains were grown and processed as for D). Dashes indicate cell
800 boundaries and the scale bar is 5 μm.
801
802